



BRNO UNIVERSITY OF TECHNOLOGY

VYSOKÉ UČENÍ TECHNICKÉ V BRNĚ

CENTRAL EUROPEAN INSTITUTE OF TECHNOLOGY BUT

STŘEDOEVROPSKÝ TECHNOLOGICKÝ INSTITUT VUT

LOW-TEMPERATURE PLASTIC DEFORMATION OF BCC METALS WITH INTERNAL MAGNETIC ORDER

NÍZKOTEPLTNÍ PLASTICKÁ DEFORMACE BCC KOVŮ S VNITŘNÍM MAGNETICKÝM USPOŘÁDÁNÍM

SHORT DOCTORAL THESIS

TEZE DIZERTAČNÍ PRÁCE

AUTHOR

AUTOR PRÁCE

Ing. Jakub Holzer

SUPERVISOR

ŠKOLITEL

doc. Ing. Roman Gröger, Ph.D. et Ph.D.

BRNO 2022

Klíčová slova

α -Fe, chrom, nízkoteplotní plastická deformace, dvojčatění, antidvojčatění, anomální skluz, vnitřní magnetické uspořádání

Keywords

α -Fe, chromium, low-temperature deformation, twinning, antitwinning, anomalous slip, internal magnetic order

Místo uložení práce

Originál Ph.D. práce je uložen na studijním oddělení Středoevropského technologického institutu Vysokého učení technického v Brně.

Purkyňova 123, 612 00, Brno, Česká Republika

©Jakub Holzer, 2022
ISBN 80-214-
ISSN 1213-4198

Contents

1	Introduction	5
1.1	Low-temperature plastic deformation of bcc metals	7
2	Magnetic states of Cr after plastic deformation	12
2.1	Prediction of magnetically dead regions in Cr	12
2.2	Simulated neutron diffraction patterns of magnetically dead regions .	13
3	Discussion	17
3.1	Magnetic measurements on α -Fe	17
3.2	Compression tests on Cr	17
3.3	Compression tests on α -Fe	19
4	Summary and future work	20
	Bibliography	22
5	Curriculum Vitae	27
6	Abstract	29

1 Introduction

The low temperature plastic deformation of magnetic body-centered cubic (bcc) metals α -Fe and Cr has received very little attention despite the fact that they are essential ingredients in dilute ferroalloys $\text{Fe}_{1-x}\text{Cr}_x$, which are model materials for the development of ferritic/martensitic steels with applications in the design of fusion reactors [1]. The mechanisms governing the plastic deformation of bcc metals are very different from those of close-packed metals such as Al, Cu, or Au [2]. Yet, the plastic behavior of the latter metals is still used as a paradigm for the understanding the deformation behavior of all crystalline materials. The experiments required to elucidate the deformation mechanisms are extremely challenging as they require single crystals of considerable size and very high purity, whose preparation is complicated, especially those of α -Fe. The preparation of iron single crystals is problematic due to the structural transition from the high-temperature ferritic body-centered cubic phase to the austenitic face-centered cubic (fcc) phase and again the low-temperature ferritic bcc phase, the latter of which remains stable to 0 K. The situation with Cr is very different. Large enough single crystals of high purity have been available commercially for many years. However, they often contain internal defects such as holes and voids.

To the best of our knowledge, only two old experimental papers looking at some aspects of the low-temperature plastic behavior of pure Cr single crystals can be found in the literature [3, 4]. Greiner [3] reported wavy slip traces in chromium deformed at room temperature and suggested that it is caused by the operation of multiple slip systems. He also asserts, that the deformation mechanism is similar to that of α -Fe. Reid et al. [4] state that the slip is restricted to thin regions sheared by the $\{110\}\langle 111 \rangle$ systems below 130 K and confirms Greiner's observation of the wavy slip above 195 K, which is explained as alternating slip on planes belonging to the $\langle 111 \rangle$ zone. Furthermore, the twinning systems were found to be of the $\{112\}$ type.

The existing knowledge about the behavior of pure α -Fe owes much to detailed experiments by Aono et al. [5]. What α -Fe and Cr, together with other metals of groups 5 and 6, have in common is the non-closed-packed bcc structure in which the screw dislocations possess non-planar cores. Their movement under stress is very limited at low temperatures [6], which results in steel increase of the flow stress as the temperature is lowered. Unlike other bcc metals, Cr and α -iron are both metals with internal magnetic order. α -iron is a well-known ferromagnetic material. In contrast, the magnetic state of chromium is characterized by antiferromagnetic spin-density waves [7], which is a more complex magnetic state than that of other, simple antiferromagnets such as metal oxides MnO, FeO and NiO. The spin density

waves in chromium are incommensurate with the structural unit cell, whereby their wavelength is not an integer multiple of the lattice parameter.

The properties of magnetic materials are commonly described by the hysteresis curve and parameters obtained from it. The hysteresis curve (or loop) is a graphical representation of the relationship of the magnetic flux density B (or magnetization M) and magnetizing field H . The hysteresis curves are often measured in the vibrating sample magnetometer by applying the magnetic field across the sample and measuring the magnetic moment induced in the specimen in the direction of the magnetizing field by vibrating the specimen near a set of measurement coils.

The magnetic hysteresis arises in the material when an external magnetic field is applied and magnetic moments are aligned with the field. Upon removal of the magnetizing field, part of the magnetic order will remain. Once the material is magnetized, it will stay that way unless acted upon by external forces such as temperature or magnetizing field applied in the opposite direction. The hysteresis curve is characterized by several parameters. The saturation magnetization in the positive direction M_s or in the negative direction $-M_s$ are estimated simply as maximum value of magnetization in saturation¹. The remanence, alternatively remanent magnetization, M_r is the magnetization that remains in the material when the external magnetic field is removed. In the hysteresis curve, this value is found at the intersection of the vertical axis with the curve. Similarly, the magnetic coercivity, alternatively coercive field, H_c characterizes the ability of the material to retain its magnetization in demagnetizing fields. The value of coercivity is found at the intersection of the horizontal axis with the hysteresis loop. Magnetic materials are often characterized as magnetically soft or hard. Magnetically soft materials have typically very low coercivity, low remanence, and small area enclosed by the curve. Due the low remanence, the material will practically demagnetize after the magnetizing field is turned off and the hysteresis losses are very small. On the other hand, magnetically hard materials have high coercivity, high remanence, and large area of the hysteresis loop. They will retain a large part of magnetization after the magnetizing field is removed and, therefore, they are used as permanent magnets.

The effects of the elastic deformation on the magnetic properties of materials have been known for a long time. The effect of residual stress, and generation of new pinning sites and their effect on magnetization curves were discussed in depth by Makar et al. [8]. They also argue that the residual stress left in the material after plastic deformation is not as important as the generation of new pinning sites, which arrest or hinder the movement of magnetic domains. They can be in the form of dislocations, dislocation clusters, interfaces (such as twin boundaries), or secondary phase particles [9]. The level of plastic deformation can be also correlated with the coercive field H_c . With increasing deformation, the coercive field increases in both single crystals and polycrystals. However, the initial value is larger in the case of polycrystals due to the presence of grain boundaries [10]. The effect of internal stress on magnetism and vice versa can be also explored by simulations and is often the only way to study magnetism at the smallest scales. Bienvenu et al. [11], for example,

¹Saturation is reached when the increasing magnetizing field no longer increases the magnetization. Microscopically this is achieved when all magnetic dipoles are aligned with the magnetizing field.

suggests that in chromium, the $1/2\langle 111 \rangle$ dislocations shearing the crystal would produce magnetic faults. In order to remove this fault, another dislocation of the same type would have to be present, which creates a super-dislocation with the $\langle 111 \rangle$ Burgers vector. This theoretical prediction has, however, not been experimentally proven.

1.1 Low-temperature plastic deformation of bcc metals

The plastic deformation of bcc metals is governed by the motion of $1/2\langle 111 \rangle$ screw dislocations [12]. Many atomistic simulations and Density Functional Theory (DFT) studies of bcc metals made in the past three decades have provided ample evidence that the cores of these dislocations are non-planar [13–15], which gives rise to phenomena that do not occur in close-packed structures.

A schematic representation of the spreading of the core of $1/2[111]$ screw dislocation on three $\{110\}$ planes in the zone of $[111]$ slip direction is shown in Fig. 1.1. Fig. 1.1(a) and 1.1(b) show by arrows the screw and edge component of the differential displacement maps, respectively.

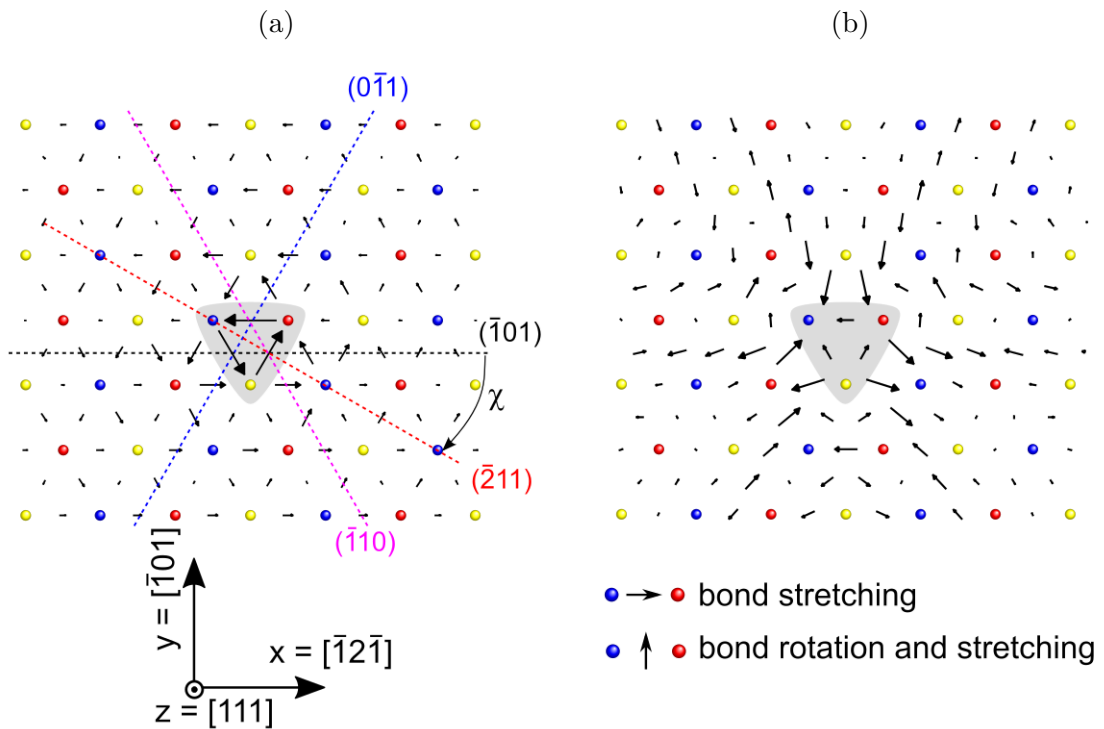


Figure 1.1: (a) screw component of the core spreading of a $1/2[111]$ screw dislocation. The arrows represent the relative displacement of a pair of atoms in the direction perpendicular to the plane of the figure. (b) edge component of the core spreading of $1/2[111]$ dislocation. The arrows here represent the relative displacement in the plane of the figure and are magnified 10x. The χ in (a) represents the angular deviation of the maximum resolved shear stress plane to the $(\bar{1}01)$ plane.

The differently colored atoms in Fig. 1.1 belong to the three successive (111) atomic layers. The magnitude of the arrows represent the relative displacement of the two atoms in the direction perpendicular to the figure's plane (Fig. 1.1(a)) or parallel (Fig. 1.1(b)). If the arrow in Fig. 1.1(b) points from one atom to another, it represents bond stretching. On the other hand, if the arrow does not point from one atom to another, the bond is partially rotated and stretched, as visualized in the bottom part of Fig. 1.1(b). Moreover, a vector sum of the edge components on any path encircling the center of the dislocation is zero, while vector sum of screw components along any such path is the Burgers vector of the dislocation.

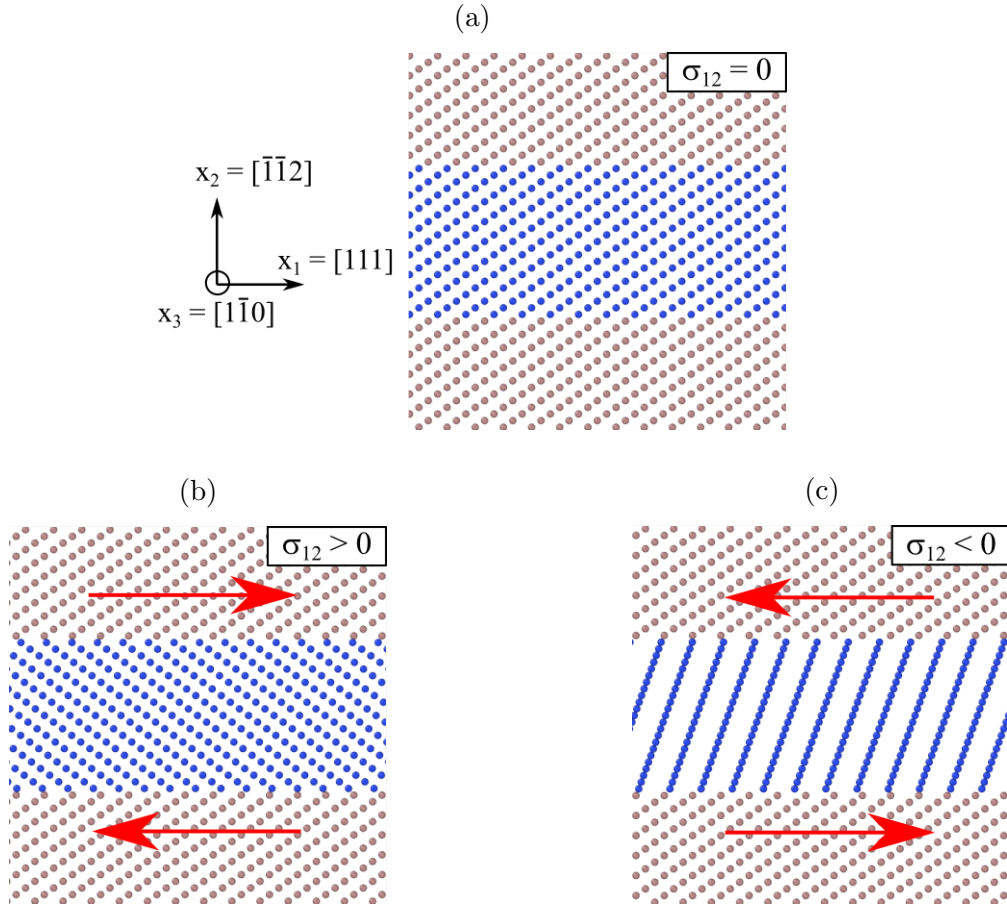


Figure 1.2: Illustration of the deformation of the perfect bcc lattice (a) in the twinning sense (b) and in the antitwinning sense (c).

The movement of the dislocation with the non-planar core cannot occur without the transformation of the core to a glissile configuration. The exact process of core transformation and movement is a subject of investigation [16]. Nonetheless, this process is thermally activated, which is why ductile-brittle transition is found in bcc metals². Another remarkable feature of the bcc lattice is the twinning-antitwinning asymmetry of the shear stress parallel to the slip direction [17]. In practice, the twinning-antitwinning asymmetry is manifested by a relatively low resistance to

²In practice, ductile-brittle transition is heavily influenced by the level of impurities in the material.

shearing the crystal on the $\{112\}$ plane in the twinning direction and higher resistance to shear in the opposite, antitwinning, direction [18]. This asymmetry has its origin in different atomic arrangements when shearing the crystal in the two opposite directions [19]. Fig. 1.2 shows a schematic illustration of the bcc lattice sheared in the twinning and antitwinning sense.

Fig. 1.2 shows different lattice deformations when shearing the crystal in $[111]$ or $[\bar{1}\bar{1}\bar{1}]$ directions along a $\{112\}$ plane. Fig. 1.2(a) is the initial bcc lattice at zero applied shear. Fig. 1.2(b) shows the structure generated by shear applied in the twinning sense, which results in a twinned structure. The remaining Fig. 1.2(c) shows deformation caused by the shear of the same magnitude applied in the antitwinning sense that results in a structure different from the twin.

Using atomistic modeling, Ito and Vitek [20] found out that shear stress parallel to the slip direction, referred to as critical resolved shear stress (CRSS) is not symmetric with respect to the change of sign of the angle χ of the maximum resolved shear stress plane (MRSSP, the plane in the zone of the slip direction with the largest resolved shear stress parallel to the slip direction). This is represented in Fig. 1.3.

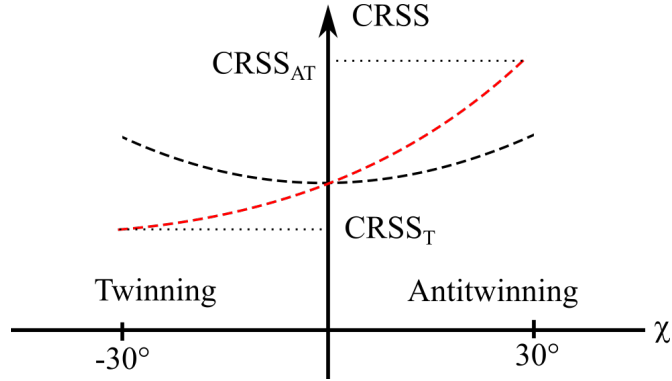


Figure 1.3: Schematic representation twinning-antitwinning asymmetry (red) for shear stress applied in various MRSSPs (angle χ) parallel to the slip direction. The black dashed curve follows the $CRSS(0)/\cos\chi$ relationship and represents a hypothetical material without the twinning-antitwinning asymmetry.

According to the Schmid law, the plastic deformation is initiated on the slip system for which the resolved shear stress parallel to the slip direction acting in this slip plane is the largest [21]. The relation between the uniaxial load represented by the stress σ , the orientation of the applied load, and the Schmid stress τ is:

$$\tau = m\sigma, \quad (1.1)$$

where $m = \cos\chi \cos\lambda$ is the Schmid factor. Here, χ is the orientation of the MRSSP, as explained before, and λ the angle between the loading axis and the slip direction. The CRSS and the Schmid stress are related by $\tau = CRSS \cos\chi$.

Due to the crystal symmetry, the angle χ ranges from values from -30° to 30° , i.e. from $(\bar{1}\bar{1}2)$ plane to $(\bar{2}11)$ plane. Shearing the crystal in the $(\bar{1}\bar{1}2)$ plane parallel to the $[111]$ direction produces a twin shown in Fig. 1.2(b). However, applying the shear of the same magnitude but opposite direction, i.e. $[\bar{1}\bar{1}\bar{1}]$, does not produce a

twin; instead it results in the high-energy structure shown in Fig. 1.2(c). If one of the above $\{112\}$ planes is sheared in the twinning sense, the other is sheared in the antitwinning sense and vice versa. Reversing the sense of shearing on the MRSSP thus swaps the character (twinning \leftrightarrow antitwinning) on the neighboring $\{112\}$ plane.

Furthermore, due to the dislocation core being extended into three planes, the dislocation glide is affected by stresses not belonging to the slip plane. These stresses are called non-Schmid stresses [22]. The asymmetry of the CRSS with respect to the orientation of the MRSSP and its variation with the shear stresses parallel to the slip direction cause the breakdown of the Schmid law in bcc metals. The simulations also revealed that if the shear stress perpendicular to the slip plane of $1/2[111]$ dislocation is high enough, the dislocation may glide on planes with lower resolved shear stress than the most highly stressed plane. This unusual behavior is referred to as anomalous slip. While the previously mentioned phenomena are prevalent in bcc metals at low temperatures, anomalous slip has been reported only in Mo, V, W, Nb, Ta [22–26]. This proves that this behavior is not connected only to crystallography but also to details of the atomic bonding. The effect of non-glide stresses also plays an important role in the tension-compression asymmetry [27], where tension and compression stress-strain curves for single crystals with the same loading axis differ significantly. The non-planar character of the dislocation also allows for easier cross-slip of the dislocation into a $\{110\}$ plane with lower resolved shear stress parallel to the slip direction. For the above-mentioned reasons, it is clear that the prediction of plastic behavior from the yield criteria based on the Schmid law cannot effectively describe the onset of plastic deformation in bcc metals [28]. A more appropriate form was proposed by Qin and Bassani [29] and parameterized for Mo, W and Cr by Gröger et al. [30,31]. and for α -Fe by Chen [28]. The yield criterion based solely on the Schmid law, in a simple way, would take the form of Eq. (1.2):

$$\tau_{Schmid}^{\alpha} \leq \tau_{cr}^* \quad (1.2)$$

In this equation, τ_{Schmid}^{α} represents the Schmid stress acting in the slip system α and drives the dislocation in the glide plane. When it reaches the critical value of stress on the slip system α , the dislocation glide will begin. This yield criterion doesn't account for non-glide stresses. The generalized version of (1.2) yield criterion takes the form:

$$\tau^{\alpha*} = \tau_{Schmid}^{\alpha} + a_1\tau_1^{\alpha} + a_2\tau_2^{\alpha} + a_3\tau_3^{\alpha} \leq \tau_{cr}^* \quad (1.3)$$

The three terms containing a_1, a_2 and a_3 represent the stresses that modify the structure of the dislocation core (so-called non-glide stresses). The term τ_1^{α} is the stress acting parallel to the slip direction but applied in a different $\{110\}$ plane. This term introduces the twinning-antitwinning asymmetry of the critical resolved shear stress. The τ_2^{α} and τ_3^{α} are shear stresses perpendicular to the slip direction (they do not affect the Peach-Koehler force acting on the dislocation). The coefficients (a_1, a_2, a_3 and τ_{cr}^*) represent adjustable parameters determined by atomistic calculations [30]. The form (1.3) describes accurately the onset of plastic deformation in non-magnetic materials and magnetic materials (α -Fe [28]), where the changes of magnetism do not affect yielding. In general, the presence of internal magnetic order requires further generalization of the yield criterion described by (1.3). In the

case of bcc metals, only chromium and α -iron show internal magnetic order. We suggest that the extended form of the yield criterion for magnetic materials takes the form:

$$\tau^{\alpha*} = \tau_{Schmid}^{\alpha} + a_1(\mathbf{M})\tau_1^{\alpha} + a_2(\mathbf{M})\tau_2^{\alpha} + a_3(\mathbf{M})\tau_3^{\alpha} \leq \tau_{cr}^*(\mathbf{M}), \quad (1.4)$$

where the \mathbf{M} broadly represents the internal magnetic state of the material. These yield criteria are essential for the simulation of the behavior of the materials. Buchheit et al. [32] used the yield criterion published by Gröger and Vitek [30] and implemented it to polycrystalline plasticity model. A single crystal yield criterion for chromium was recently developed by Gröger and Vitek [31] based on atomistic modeling of isolated $1/2[111]$ screw dislocation. Generally, these yield criteria and fracture criteria are used extensively in applied research, and industry [33, 34].

2 Magnetic states of Cr after plastic deformation

Magnetism in chromium single crystals was investigated by the means of vibrating sample magnetometry and neutron scattering. The results show that the single- \mathbf{Q} state, where the magnetic ordering can be characterized by a single wavevector, can be prepared by the field cooling method described by Golovkin et al. [35], Werner et al. [36] and others [37–39]. The single- \mathbf{Q} state can be characterized to a certain extent by measuring the magnetic susceptibility along the three $\langle 100 \rangle$ directions of which one is parallel to the wavevector and two perpendicular to it. The magnetic susceptibility, a measure of how easily a material can be magnetized in an external magnetic field, will be lower when measured parallel to the spins. Furthermore, in the single- \mathbf{Q} state, the change of magnetic susceptibility across the spin-flip temperature T_{SF} is readily observable. The preparation of the single- \mathbf{Q} state was also verified by the magnetic neutron scattering, which shows that a majority of specimens were in the single- \mathbf{Q} state. However, less intense reflections corresponding to other spin density waves were observed. The presence of other SDWs, albeit much weaker in the intensity, suggests that the field cooling process did not fully transform the magnetic order in the specimen. The magnetic state of the field-cooled specimens that were predeformed at room temperature tend to favor the $(1 \pm \delta, 0, 0)$ spin density wave. However, the magnetic state is largely inconsistent between the specimens.

The magnetic neutron scattering of the specimens deformed at 77 K reveals that the magnetic state corresponds to the single- \mathbf{Q} state described by the $(0, 1 \pm \delta, 0)$ SDW, which would be created by field cooling in the $[010]$ direction. All three specimens deformed at 77 K were field-cooled in different $\langle 100 \rangle$ directions, and we would expect their initial state to be similar to the predeformed specimens. One could expect the final magnetic state after the plastic deformation at 77 K to be similar to the stress-cooled state, as elastic deformation precedes and is present during the plastic deformation. All of these assumptions are, however, wrong, as the final state is the perfect single- \mathbf{Q} state. To the best of our knowledge, this behavior has not been reported in the literature, and unfortunately remains poorly understood.

2.1 Prediction of magnetically dead regions in Cr

We have made further magnetic neutron scattering experiments to test the hypothesis of Bienvenu et al. [11], that the glide of the $1/2[111]$ screw dislocations on $\{110\}$,

$\{112\}$ and $\{123\}$ atomic planes creates magnetic faults. This is the result of the magnetic frustration, which is due to the fact that the $1/2[111]$ vector does not connect identical spins (is not the translation vector from the point of view of the magnetic structure). The fault region is characterized by a negligible magnitude of the atomic magnetic moment. Furthermore, a dislocation creating such magnetic fault would have to be followed by another dislocation of the same type to close the magnetic fault, making it effectively a superdislocation with $\langle 111 \rangle$ Burgers vector. We have simulated the expected magnetic neutron diffraction patterns by calculations based on the DFT results obtained by Bienvenu et al. [11]. The infinite magnetic fault is shown Fig. 2.1, where antiferromagnetic order sets in away from the fault. Fig. 2.1(a) shows an infinite magnetic fault in chromium along the $\{110\}$ plane, where the differently sized circles represent a different magnitude of magnetic moment. The touching circles have value of $1.1\mu_B$, while the smallest ones have value of $0.2\mu_B$. Similarly, Fig. 2.1(b) shows an infinite magnetic fault on the $\{112\}$ plane, but in this case, the smallest circles represent a zero magnetic moment.

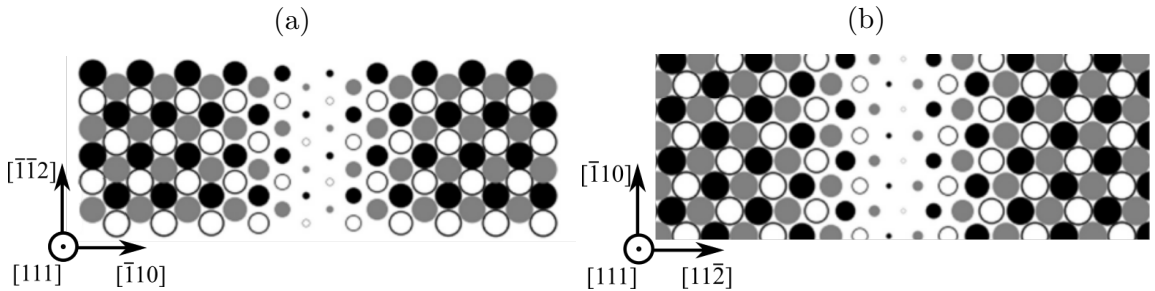


Figure 2.1: Magnitude of the magnetic moments in an infinite magnetic fault in a form of differently sized circles. Magnetic fault on: (a) $\{110\}$ plane, (b) $\{112\}$ plane. The touching circles represent the magnetic moment of $1.1\mu_B$, whereas the smallest circles represent value of $0.2\mu_B$ and zero in (a) and (b), respectively. Figures adapted from Bienvenu et al. [11].

2.2 Simulated neutron diffraction patterns of magnetically dead regions

The simulation assumes the spin direction along $[010]$, which corresponds to the LSDW (Longitudinal Spin Density Wave) single- \mathbf{Q} state characterized by the $(0, 1 \pm \delta, 0)$ fundamental spin density wave. Therefore, the simulation describes the final magnetic state of the specimen deformed at 77 K. The simulation cell with the magnetic fault on the $\{110\}$ comprises of 120 atoms, which is replicated $16 \times 16 \times 2$ times in the x, y, z direction, respectively. The total number of atoms is 61 440 atoms. Similarly, the simulation of the magnetic fault on the $\{112\}$ plane comprises also of 120 atoms replicated $20 \times 20 \times 2$ times along the three axes. The total number of atoms is then 96 000. The atomic positions and the magnitudes

of magnetic moments were obtained from DFT simulation of Bienvenu et al. [11], kindly provided to us by E. Clouet. It is imperative to mention that both the DFT and the simulation of neutron diffraction patterns are calculated at 0 K, while the experimental data obtained at PSI are measured at higher temperatures. Although we compare the same SDW (Spin density wave) states, the temperature difference may play a role. Due to crystal symmetry, all $\{110\}$ planes are equivalent. Therefore, we have considered all these six $\{110\}$ planes to simulate the magnetic neutron diffraction patterns from the faulted atomic block. The simulated magnetic neutron scatterings from the $\{110\}$ planes are shown in Fig. 2.2. Similarly, twelve $\{112\}$ planes exist in bcc crystals that are all crystallographically equivalent. The simulations of magnetic neutron diffraction patterns were thus made by assuming that the magnetic fault may occur on all these planes. The simulated magnetic scattering patterns from $\{112\}$ planes are shown in Fig. 2.3.

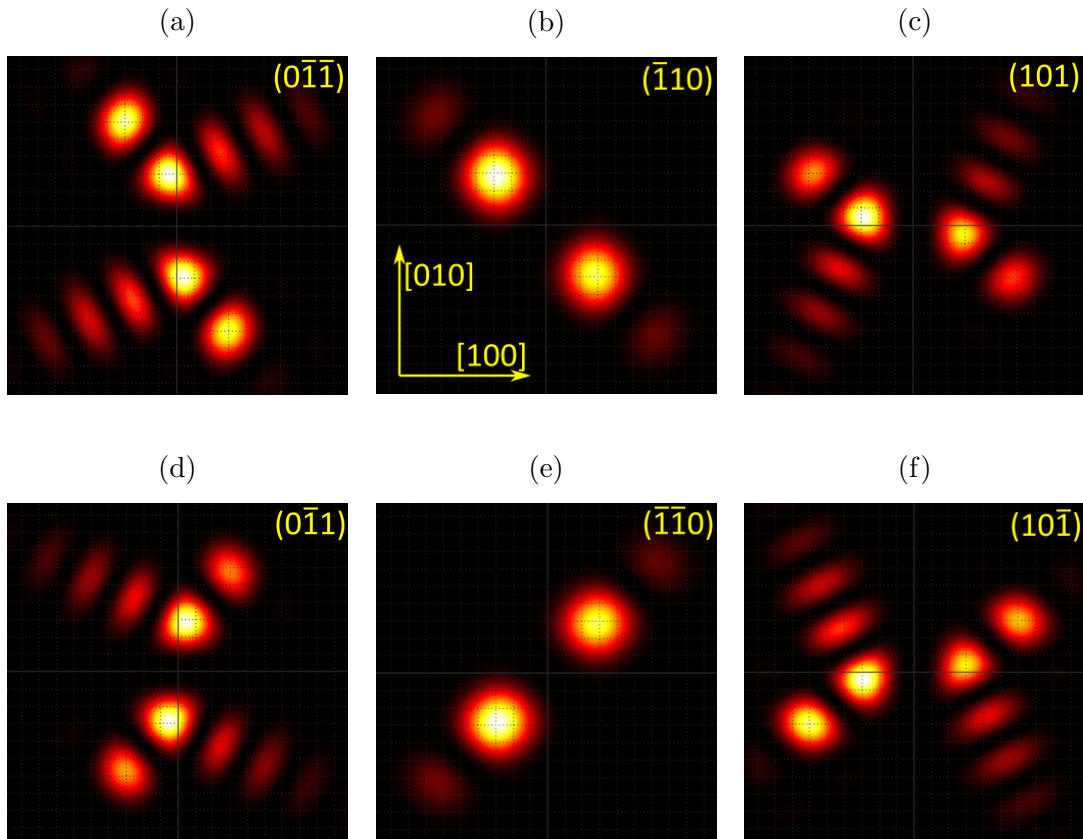


Figure 2.2: Simulations of symmetry-related diffraction patterns for $\{110\}$ magnetic fault. Spin direction is $\mathbf{S} = [010]$, wavevector of SDW $\mathbf{Q} = [010]$ (i.e. LSDW state). Magnetic fault on: (a) $(0\bar{1}\bar{1})$ plane, (b) $(\bar{1}10)$ plane, (c) (101) plane, (d) $(0\bar{1}\bar{1})$ plane, (e) $(\bar{1}\bar{1}0)$ plane, (f) $(10\bar{1})$ plane.

Fig. 2.4(b) and 2.4(c) show superpositions of the neutron magnetic scattering of all $\{110\}$ and $\{112\}$ atomic planes, respectively, that were made with equal weights assigned to the individual diffractions from all $\{110\}$ and $\{112\}$ planes, as shown in Fig. 2.2 and 2.3, respectively. Fig. 2.4(a) shows the data from the neighborhood of

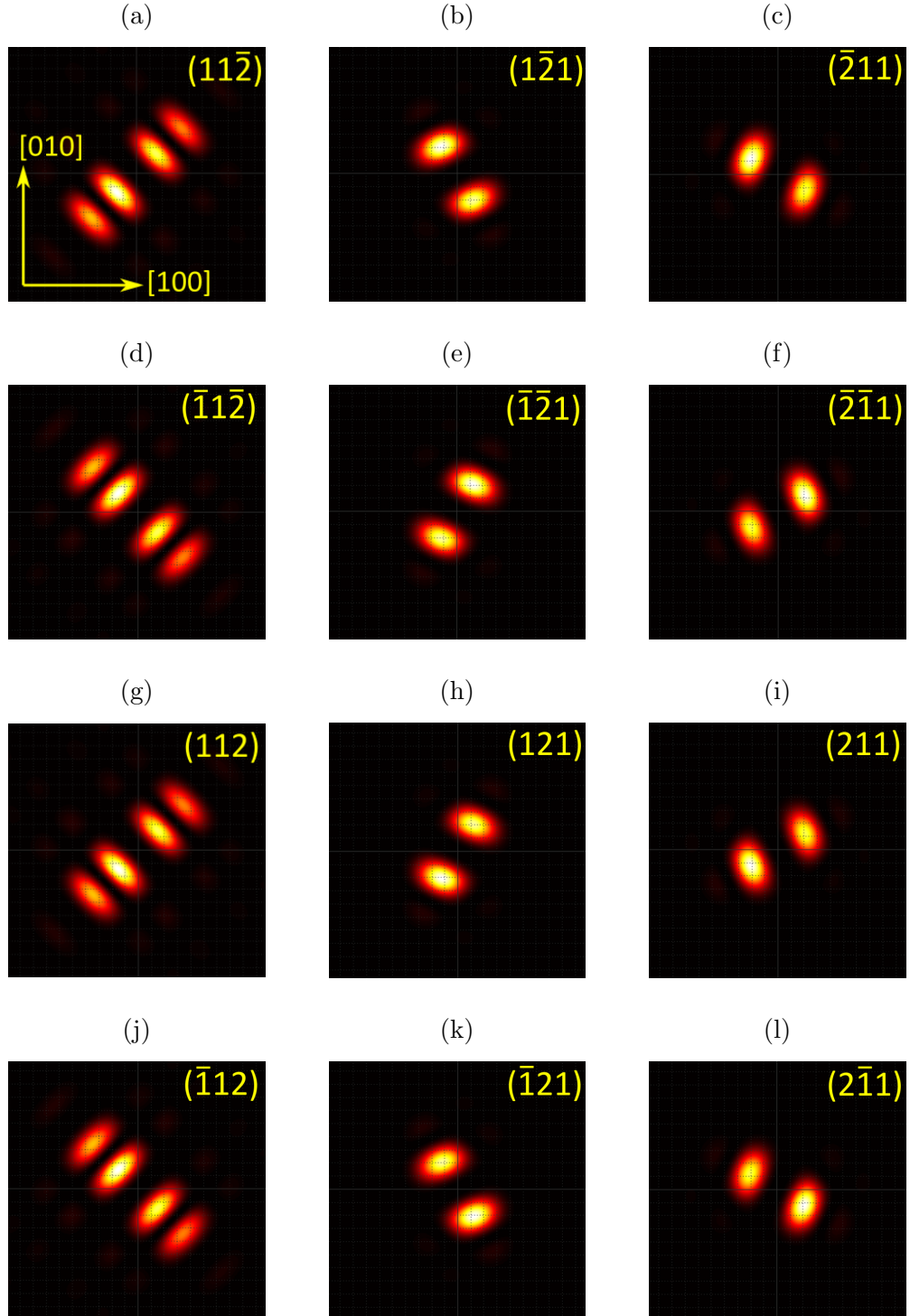


Figure 2.3: Simulation of symmetry-related diffraction patterns for $\{112\}$ magnetic faults. Spin direction is $\mathbf{S} = [010]$, wavevector of SDW $\mathbf{Q} = [010]$ (i.e. LSDW state). Magnetic faults on: (a) $(11\bar{2})$ plane, (b) $(1\bar{2}1)$ plane, (c) $(\bar{2}11)$ plane, (d) $(\bar{1}\bar{1}\bar{2})$ plane, (e) $(\bar{1}\bar{2}1)$ plane, (f) $(\bar{2}\bar{1}1)$ plane, (g) (112) plane, (h) (121) plane, (i) (211) plane, (j) $(\bar{1}\bar{1}2)$ plane, (k) $(\bar{1}\bar{2}1)$ plane, (l) $(2\bar{1}1)$ plane.

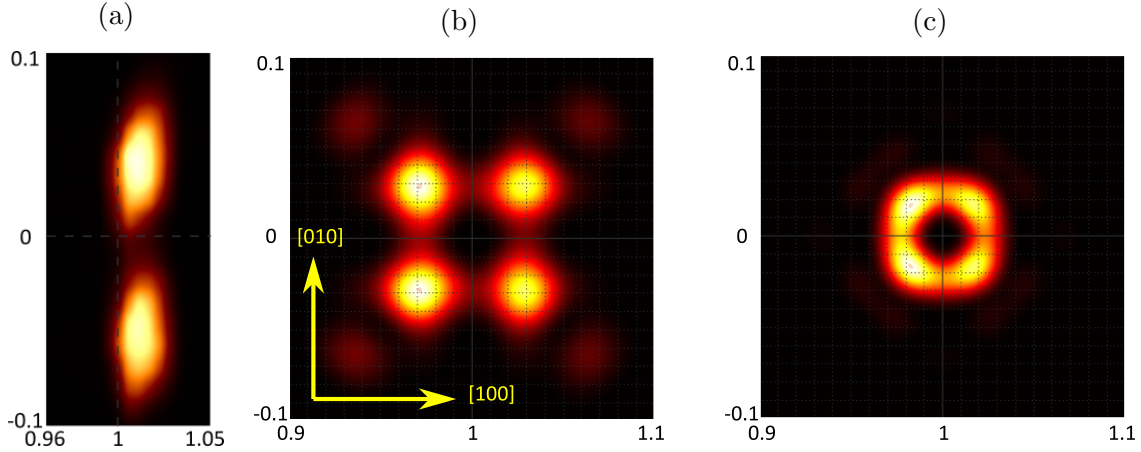


Figure 2.4: (a) Neighborhood of the $[100]$ magnetic reflection obtained from neutron magnetic scattering. Visible reflections are $[1, \delta, 0]$ and $[1, -\delta, 0]$ on the top and bottom, respectively. Superposition of all simulated symmetry-related (b) $\{110\}$ and (c) $\{112\}$ magnetic diffraction patterns described in the text. Spin direction is $\mathbf{S} = [010]$, SDW wavevector $\mathbf{Q} = [010]$, i.e. LSDW state.

$[100]$ magnetic reflection that I have measured using magnetic neutron scattering at PSI at 10 K on the PSI 3 specimen. In this case, we used the so-called q -scans to resolve the reflections better. Q -scans are done with the 1D detector and acquired as line scans in the reciprocal space. This measurement is comprised of seventeen line scans from $0.96H$ to $1.04H$ ($H = [100]$), each line spanning from $-0.14K$ to $0.14K$ ($K = [010]$) at $L = 0$ ($L = [001]$). The reflections in Fig. 2.4(a) belong to the $[1, \delta, 0]$ and $[1, -\delta, 0]$ on the top and bottom, respectively.

It is evident that the simulated diffraction patterns do not agree with the experimental measurements. The reason can be that not all symmetry-related faults are present with the same probability in the studied volume. In this case, different weights would have to be assigned to the patterns in Fig. 2.2 and 2.3. However, it is not clear how these weights could be determined from experiments. The volume fraction of the magnetic faults to the remaining material would likely be very small and difficult, if not impossible, to measure.

Furthermore, the TEM study of the anomalous slip in Cr deformed at 77 K did not present any evidence of superdislocations with $\langle 111 \rangle$ Burgers vectors as hypothesized by Bienvenu et al. [11]. So far, we have not found any evidence that would support their conclusion, that deformed Cr single crystals contain magnetically dead regions separating dislocations with the same Burgers vectors. The stresses around the dislocation affect the magnetic ordering, but they do not seem to be large enough to produce magnetic faults as predicted in their paper.

3 Discussion

3.1 Magnetic measurements on α -Fe

The hysteresis curves measured by VSM on polycrystalline α -Fe showed, as anticipated, that with more plastic deformation imposed on the material, the number of domain wall pinning sites increases. This effect is dominant when the probing magnetic field is parallel with the deformation axis and results in increasing slope of the hysteresis curve (larger susceptibility relative to unstressed specimens). When the direction of the probing field is perpendicular to the deformation axis, this effect is smaller and the slope of the hysteresis curve changes in the opposite direction (smaller susceptibility). Furthermore, if the step of the VSM measurement is fine enough, it is possible to observe the release of domain walls from the pinning sites.

The Kerr microscopy revealed that magnetic domains in single-crystalline specimens are larger compared to those in polycrystalline specimens. Interestingly, twins in the material create effective barriers for the domains in some cases, but they may also serve as nucleation sites for other magnetic domains. Lai et al. found that twins in NiMnGa shape memory alloy transfer the magnetic domains through the twins according to the rotation of crystal lattice in the twin [40]. On the other hand, if the twins are very thin (tens to low hundreds of nm), the magnetic domain can pass through the domain structure [41]. Nonetheless, the effects observed here might appear only near the surface, since the depth resolution of Kerr microscopy is approximately 50 nm [42]. Bozorth [43] states that the maze-like domain structure is characteristic of a deformed material and the tree-like domain structure is characteristic of an undeformed material. Nonetheless, both specimens were strained, but at different temperatures and to different amounts. Fe-mono-1 specimen was strained at RT to approx. 6% and Fe-mono-2 specimen was prestrained to 1.7% at RT and subsequently deformed at 77 K to further 2.5%. The results may indicate, that low-temperature slip have larger effect on magnetic domains than slip at RT.

3.2 Compression tests on Cr

The mechanism of low-temperature plastic deformation of UHV-annealed high-purity Cr single crystals depends on the orientation of the applied load as well as on whether the sample was predeformed at room temperature, thus creating mobile dislocation network. The samples compressed close to the [001] direction exhibit homogeneous slip on slip systems with the highest Schmid factors. In this region, pre-deformation does not alter the mechanism of plastic deformation. Similar behavior

is observed for the specimen 7* predeformed at room temperature and subsequently compressed at 77 K in the center-triangle direction closer to the $[001]$ - $[011]$ edge. However, specimen 3, which was not predeformed at room temperature, exhibited a combination of composite slip and twinning. The specimen 4* deformed in the direction corresponding to the center of the stereographic triangle showed anomalous slip on the $(0\bar{1}1)$ plane. For loading directions close to the $[011]$ - $[\bar{1}11]$ edge of the stereographic triangle, the specimens deformed predominantly by twinning on the $\{112\}\langle 111\rangle$ systems, irrespective of whether or not they were predeformed at room temperature. The specimens that fractured by cleavage also exhibited the formation of twins on $\{112\}$ planes sheared in the antitwinning sense. The intersections of twins were found to lead to the nucleation of cracks and subsequent failure by cleavage. Our results agree with Marcinkovsky and Lipsitt [44], who state that twins in chromium are of the $\{112\}\langle 111\rangle$ type. Sameljuk et al. [45] states that cleavage is along $\{100\}$ planes and delamination occurs along $\{112\}$, which is also in agreement with our observations.

The anomalous slip in the samples compressed in the direction corresponding to the center of the stereographic triangle was further reconciled using bright-field STEM imaging in the $[0\bar{1}1]$ zone combined with the $\mathbf{g} \cdot \mathbf{b}$ analysis in six different diffraction conditions. They reveal the presence of intersecting $1/2\langle 111\rangle$ screw dislocations. The stability of this junction at high stresses and low temperatures was further investigated by molecular statics simulations employing the recently developed BOP for Cr in the non-magnetic state. This state-of-the-art model that treats Cr as non-magnetic metal is applicable to the triple- \mathbf{Q} state of our samples. It contains a large number of magnetic domains with all three $\langle 100\rangle$ orientations of the SDW wavevector \mathbf{Q} , which results in magnetically isotropic state above a certain length scale corresponding to the size of magnetic domains. The atomistic simulations show that the intersecting $1/2[111]$ and $1/2[\bar{1}\bar{1}\bar{1}]$ screw dislocations spontaneously form the $[100]$ screw junction, as expected from linear elasticity. More importantly, the application of external load in the $[\bar{2}38]$ center-triangle direction shows that this junction remains stable up to very high stresses, where the stored energy is relaxed by moving the dislocation network on the common $(0\bar{1}1)$ plane. A different slip plane is predicted from atomistic simulations on single dislocations, and thus the simulations of dislocation junctions are necessary to understand the mechanism of anomalous slip. Instead, interactions between dislocations play an essential role and lead to the formation of strong $\langle 100\rangle$ junctions that cannot be easily broken by the external load. Our results thus provide evidence that the anomalous slip in Cr is governed by the co-planar double slip model proposed originally by Matsui and Kimura [46].

Similar experimental results were reported by Hsiung et al [47]. in molybdenum at room temperature with the high strain rate of 1 s^{-1} or by Louchet and Kubin [48] in niobium at 50 K. According to the literature, anomalous slip takes place only in pure metals and is suppressed by impurities. Bressers and Creten [24] investigated anomalous slip in vanadium single crystals with different levels of oxygen content (from 24 to 810 at. ppm). Their results shown that the morphology of surface markings belonging to anomalous slip change from finely distributed to coarse and more separated surface markings.

3.3 Compression tests on α -Fe

The analysis of compression tests on the polycrystalline specimens with large grains reveals that the primary deformation mechanism at 77 K is twinning regardless of the orientation of the loading axis. Apart from SEM and EBSD analysis, the twinning is also evident from the stress-strain curve that displays many load drops caused by the nucleation of twins. No slip markings were observed in the polycrystalline specimens, that were deformed at 77 K with or without predeformation at room temperature.

Furthermore, all the analyzed twins were produced by twinning shear, even though, in many cases, the Schmid factor was larger for twinning systems sheared in the antitwinning shear. The reason for their non-existence is attributed to a large σ_{AT}/σ_T ratio that favors twin formation on the $\{112\}$ planes subjected to twinning shear. No twins were observed to form on $\{112\}$ planes sheared in the antitwinning sense. We have, however, found one $(321)[1\bar{1}\bar{1}]$ lamella sheared in the twinning sense.

The compression tests on the single-crystalline specimens did not reveal any slip traces on the surface, which suggests that the specimens deformed by homogeneous slip. This behavior is, however, different from what Aono et al. [5] reported on approx. 1 mm single crystals in compression. He reported a combination of cleavage and twinning, while our results suggest homogeneous slip. We attribute this difference to different purity of tested specimens. Allen et al. [49] reported macroscopic slip on $(\bar{3}12)[111]$ and $(\bar{1}01)[111]$ systems in tension at 77 K. Altshuler and Christian [50] report compression tests at 77 K in both polycrystalline and single-crystalline specimens. In case of polycrystalline specimens with the mean grain diameter of 0.013 mm, they report the yield stress of approximately 690 MPa. This is in disagreement with yield stress measured on our specimen, which is approx. 140 MPa. This discrepancy can be at least partially explained by their less pure material (194 wt. ppm of impurities in their specimen vs 66 wt. ppm in our specimen), smaller grain size and slightly faster strain rate, which would cause larger yield stress. Furthermore, the reported stress-strain curves of their polycrystalline specimen do not show load drops associated with twinning. The loading axis of their single crystal specimens was $[\bar{1}49]$, which is approx. 2.5° from $[\bar{4}1126]$ loading axis of our single crystal specimens. Single crystals reported in our work are also more pure than those used by Altshuler and Christian. Nevertheless, the reported yield stress of 50 MPa is almost identical for specimen deformed at RT. However, their specimen shows some strain hardening, whereas ours show almost continual room temperature creep. Comparing the specimens tested at 77 K, Altshuler and Christian report yield stress of approx. 540 MPa, whereas the yield stress of our specimen was approx. 460 MPa. This discrepancy can be again explained by chemical purity of the specimens, prestrain of our specimens at RT, and about twice slower strain rate used in our experiments.

4 Summary and future work

Following are the main achievements of this work that were discussed in detail in the previous chapters.

- Anomalous slip in chromium single crystals was demonstrated for the first time. The presence of $\langle 100 \rangle$ dislocation junctions was proven by the $\mathbf{g} \cdot \mathbf{b}$ analysis on micrographs acquired in TEM. Furthermore, the anomalous slip in Cr is confirmed by atomistic simulations done in our group, which show that it is governed by the co-planar double slip process of Matsui & Kimura [51] and Louchet & Kubin [48].
- The reason for the presence or absence of twins created by antitwinning shear in chromium and α -iron was elucidated. The presence of twins created by antitwinning shear depends on the ratio of stresses necessary to create multi-layer stacking faults in the antitwinning and twinning direction by uniform shear. This ratio is approximately twice as large for α -Fe compared to chromium, which explains why twins in α -Fe only form by the twinning shear.
- Misoriented lamellae on $\{123\}$ planes were observed in α -iron. However, these are scarce due to higher stresses necessary to move dislocations on $\{123\}$ planes compared to dislocations on $\{112\}$ planes. Nonetheless, according to calculations, shear stress required to nucleate these faults on $\{123\}$ planes by the twinning shear is smaller compared to the shear stress necessary to create a $\{112\}$ twin by antitwinning shear.
- Plastic deformation of Cr single crystals at 77 K promotes a single- \mathbf{Q} state with the spin density wave along closest $\langle 100 \rangle$ crystal direction. This phenomenon has not been reported in the literature so far.
- Our neutron diffraction results do not support the conclusion of Beinvenu et al. [11], that dislocations in chromium give rise to magnetic faults. However, neutron diffraction is a statistical method and thus magnetic faults may not be found in the interaction volume with sufficient density to be revealed in diffraction patterns. So far, we have not found any evidence that would support their hypothesis.
- Based on results presented in this thesis, the effect of internal magnetic order of Cr and α -Fe seems to have little effect on their deformation properties within the first 5% of their plastic deformation. The only result that would support the opposite is the inexplicable increase of the yield stress of chromium

specimen that had the spin density wave wavevector oriented close to the loading axis. On the other hand, the effect of plastic deformation on internal magnetic structure of Cr and α -Fe is severe.

Different propensity to twin formation and its non-existence when the shear is applied in the antitwinning sense is sometimes regarded as a consequence of different elastic anisotropy. The Zener's anisotropy ratio of α -Fe at room temperature is approx. 2.4 [52], whereas that for alkali metals Li, Na and K are 8.8, 8.2 and 6.4 respectively [53–55]. Both α -Fe and alkali metals exhibit large anisotropy, while other bcc metals show rather small values of Zener's ratio. In particular, Cr, Ta, W, Mo, Nb and V have Zener's ratio of 0.69, 1.58, 1.00, 0.81, 0.51 and 0.79, respectively [56–58]. The anisotropy indices seem to correlate with σ_{AT}/σ_T ratios computed in Ref. [59]. However, twinning is governed by the glide of twin boundary dislocations, whose cores are not described by elasticity. From this point of view, anisotropic elasticity cannot govern the glide of these dislocations, albeit it may somewhat affect this mechanism.

This work suggests that magnetic ordering does not play a major role in the twinning of bcc metals. Future research should focus on elucidating the deformation mechanisms of alkali metals, since the 5th and 6th group bcc metals and iron have been studied quite extensively. The lack of data on alkali metals stem from their high reactivity and thus difficult handling and testing. The only recent study on alkali metals was published by Sedlatschek et al. [60] who studied Li in tension, but did not focus on operative slip systems. Despite the nucleation and growth of twins in bcc metals have been simulated a number of times, in-situ experimental studies of twin formation is still lacking. In particular, it is still unclear how twin embryos originate. Future research could also focus on Fe-Cr alloys and their properties, which are one of the candidate materials considered for the design of fusion reactors [61, 62].

Bibliography

- [1] M. J. Paul, V. M. Muthaiah, S. Mula, Yttria-reinforced Fe-Cr ferritic alloy-based nanocomposites for fusion reactor structural applications, *Metall. Mater. Trans. A* 52 (2021) 627–643.
- [2] J. W. Christian, Some Surprising Features of the Plastic Deformation of Body-Centered Cubic Metals and Alloys, *Metall. Trans. A* 14 (1983) 1237–1256.
- [3] E. S. Greiner, Slip Markings in Chromium, *JOM* 2 (1950) 891–892.
- [4] C. N. Reid, A. Gilbert, G. Hahn, Dislocation and deformation modes in chromium single crystals, *Trans. Metall. Soc. AIME* 239 (1967) 467–473.
- [5] Y. Aono, E. Kuramoto, K. Kitajima, Plastic Deformation of High-Purity Iron Single Crystals, *Rep. Res. Inst. Appl. Mech.* 29 (1981) 127–189.
- [6] F. Louchet, L. P. Kubin, D. Vesely, In situ deformation of bcc crystals at low temperatures in a high-voltage electron microscope: Dislocation mechanisms and strain-rate equation, *Philos. Mag. A* 39 (1979) 433–454.
- [7] E. Fawcett, Spin-Density-Wave Antiferromagnetism in Chromium, *Rev. Mod. Phys.* 60 (1988) 209–283.
- [8] J. M. Makar, B. K. Tanner, The effect of plastic deformation and residual stress on the permeability and magnetostriction of steels, *J. Magn. Magn. Mater.* 222 (2000) 291–304.
- [9] K. M. Krishnan, Magnetism and microstructure: the role of interfaces, *Acta Mater.* 47 (1999) 4233–4244.
- [10] S. Takahashi, J.-I. Echigoya, Z. Motoki, Magnetization curves of plastically deformed Fe metals and alloys, *J. Appl. Phys.* 87 (2000) 805–813.
- [11] B. Bienvenu, C. C. Fu, E. Clouet, Impact of magnetism on screw dislocations in body-centered cubic chromium, *Acta Mater.* 200 (2020) 570–580.
- [12] V. Vitek, Core Structure of Screw Dislocations in Body-Centred Cubic Metals: Relation to Symmetry and Interatomic Bonding, *Philos. Mag.* 84 (2004) 415–428.
- [13] M. S. Duesbery, The dislocation core and plasticity, *Dislocations in Solids* 8 (1989) 67–173.

- [14] M. S. Duesbery, V. Vitek, D. K. Bowen, P. B. Hirsch, The Effect of Shear Stress on the Screw Dislocation Core Structure in Body-Centred Cubic Lattices, *Proc. R. Soc. Lond. A* 332 (1973) 85–111.
- [15] S. L. Frederiksen, K. W. Jacobsen, Density Functional Theory Studies of Screw Dislocation Core Structures in Bcc Metals, *Philos. Mag.* 83 (2003) 365–375.
- [16] T. Suzudo, T. Onitsuka, K. Fukumoto, Analyzing the Cross Slip Motion of Screw Dislocations at Finite Temperatures in Body-Centered-Cubic Metals: Molecular Statics and Dynamics Studies, *Model. Simul. Mater. Sci. Eng.* 27 (2019) 064001.
- [17] V. Vitek, R. C. Perrin, D. K. Bowen, The core structure of $1/2$ (111) screw dislocations in bcc crystals, *Philos. Mag.* 21 (1970) 1049–1073.
- [18] J. Wang, Z. Zeng, M. Wen, Q. Wang, D. Chen, Y. Zhang, P. Wang, H. Wang, Z. Zhang, S. X. Mao, Anti-twinning in nanoscale tungsten, *Sci. Adv.* 6 (2020) 1–8.
- [19] M. S. Duesbery, V. Vitek, Plastic anisotropy in bcc transition metals, *Acta Mater.* 46 (1998) 1481–1492.
- [20] K. Ito, V. Vitek, Atomistic Study of Non-Schmid Effects in the Plastic Yielding of Bcc Metals, *Phil. Mag. A* 81 (2001) 1387–1407.
- [21] E. Schmid, W. Boas, Plasticity of crystals: With special reference to metals, Chapman & Hall, 1968.
- [22] R. Gröger, A. G. Bailey, V. Vitek, Multiscale Modeling of Plastic Deformation of Molybdenum and Tungsten: I. Atomistic Studies of the Core Structure and Glide of $1/2\langle 111 \rangle$ Screw Dislocations at 0 K, *Acta Mater.* 56 (2008) 5401–5411.
- [23] Y. Aono, E. Kuramoto, K. Kitajima, Fundamental Plastic Behaviors in High-Purity BCC Metals (Nb, Mo and Fe), in: R. C. Gifkins (Ed.), Strength of Metals and Alloys (ICSMA 6), Pergamon, 1982, 9–14.
- [24] J. Bressers, R. Creten, Suppression of Anomalous Slip by Oxygen Interstitials in Vanadium, *Scr. Mater.* 11 (1977) 33–36.
- [25] A. J. Garratt-Reed, G. Taylor, Stress-Strain Curves for Niobium Crystals Deformed at Temperatures below Ambient, *Philos. Mag.* 33 (1976) 577–590.
- [26] R. Gröger, Z. Chlup, T. Kuběnová, Deformation Twinning in Vanadium Single Crystals Tested in Compression at 77 K, *Mater. Sci. Eng. A* 737 (2018) 413–421.
- [27] H. Cho, C. A. Bronkhorst, H. M. Mourad, J. R. Mayeur, D. J. Luscher, Anomalous plasticity of body-centered-cubic crystals with non-Schmid effect, *Int. J. Solids Struct.* 139 (2018) 138–149.

- [28] Z. Chen, *Modelling the plastic deformation of iron*, KIT Scientific Publishing, 2013.
- [29] Q. Qin, J. L. Bassani, Non-Schmid yield behavior in single crystals, *J. Mech. Phys. Solids* 40 (1992) 813–833.
- [30] R. Gröger, V. Racherla, J. L. Bassani, V. Vitek, Multiscale Modeling of Plastic Deformation of Molybdenum and Tungsten: II. Yield Criterion for Single Crystals Based on Atomistic Studies of Glide of $1/2\langle 111 \rangle$ Screw Dislocations, *Acta Mater.* 56 (2008) 5412–5425.
- [31] R. Gröger, V. Vitek, Single Crystal Yield Criterion for Chromium Based on Atomistic Studies of Isolated $1/2[111]$ Screw Dislocations, *Int. J. Plast.* 102733.
- [32] T. E. Buchheit, C. C. Battaile, C. R. Weinberger, E. A. Holm, Multi-scale modeling of low-temperature deformation in bcc metals, *JOM* 63 (2011) 33–36.
- [33] Y. Lou, J. W. Yoon, Anisotropic yield function based on stress invariants for BCC and FCC metals and its extension to ductile fracture criterion, *Int. J. Plast.* 101 (2018) 125–155.
- [34] O. Cazacu, B. Plunkett, F. Barlat, Orthotropic yield criterion for hexagonal closed packed metals, *Int. J. Plast.* 22 (2006) 1171–1194.
- [35] V. Golovkin, V. Bykov, V. Levдик, Obtaining the "Single-Q" State of Chromium by Action of Low Temperatures in the Presence of a Magnetic Field, *ZhETF Pis. Red.* 14 (1971) 382–385.
- [36] S. A. Werner, A. Arrott, H. Kendrick, Temperature and magnetic-field dependence of the antiferromagnetism in pure chromium, *Phy. Rev.* 155 (1967) 528–539.
- [37] T. J. Bastow, R. Street, Magnetic Structures of Field-Cooled and Stress-Cooled Chromium, *Phys. Rev.* 141 (1966) 510–516.
- [38] B. C. Munday, A. R. Pepper, R. Street, Properties of chromium cooled in a magnetic field, *Braz. J. Appl. Phys.* 15 (1964) 611–612.
- [39] M. O. Steinitz, Physical properties of chromium, *J. Magn. Magn. Mater.* 60 (1986) 137–144.
- [40] Y. W. Lai, N. Scheerbaum, D. Hinz, O. Gutfleisch, R. Schäfer, L. Schultz, J. McCord, Absence of magnetic domain wall motion during magnetic field induced twin boundary motion in bulk magnetic shape memory alloys, *Appl. Phys. Lett.* 90 (2007) 192504.
- [41] B. Zhang, W. A. Soffa, Magnetic domains and coercivity in polytwinned ferromagnets, *Phys. Status Solidi A* 131 (1992) 707–725.

- [42] K. Postava, J. F. Bobo, M. D. Ortega, B. Raquet, H. Jaffres, E. Snoeck, M. Goiran, A. R. Fert, J. P. Redoules, J. Pištora, J. C. Ousset, Magneto-optical measurements of magnetization reversal in nanometer scale sputtered Fe thin films, *J. Magn. Magn. Mater.* 163 (1996) 8–20.
- [43] R. M. Bozorth, Magnetic domain patterns, *J. Phys. Radium.* 12 (1951) 308–321.
- [44] M. J. Marcinkowski, H. A. Lipsitt, The plastic deformation of chromium at low temperatures, *Acta Metall.* 10 (1962) 95–111.
- [45] A. V. Sameljuk, A. D. Vasilev, S. A. Firstov, Low Temperature Deformation and Fracture Behaviour of [100] and [110] Chromium Single Crystals, *Int. J. Refract. Met. H.* 14 (1996) 249–255.
- [46] H. Matsui, H. Kimura, Anomalous {110} Slip in High-Purity Molybdenum Single Crystals and Its Comparison with That in V(a) Metals, *Mater. Sci. Eng.* 24 (1976) 247–256.
- [47] L. L. Hsiung, On the Mechanism of Anomalous Slip in Bcc Metals, *Mater. Sci. Eng. A* 528 (2010) 329–337.
- [48] F. Louchet, L. P. Kubin, Dislocation Substructures in the Anomalous Slip Plane of Single Crystal Niobium Strained at 50 K, *Acta Metall.* 23 (1975) 17–21.
- [49] N. Allen, B. Hopkins, J. McLennan, The Tensile Properties of Single Crystals of High-Purity Iron at Temperatures from 100 to -253 °C, *Proc. Roy. Soc. A.* 234 (1956) 221–246.
- [50] T. L. Altshuler, J. W. Christian, The mechanical properties of pure iron tested in compression over the temperature range 2 to 293 K, *Philos. Trans. R. Soc. A* 261 (1967) 253–287.
- [51] H. Matsui, H. Kimura, Anomalous {110} Slip and the Role of Co-Planar Double Slip in BCC Metals, *Scr. Metall.* 9 (1975) 971–978.
- [52] H. M. Ledbetter, R. P. Reed, Elastic properties of metals and alloys, I. Iron, nickel, and iron-nickel alloys, *J. Phys. Chem. Ref. Data* 2 (1973) 531–618.
- [53] H. C. Nash, C. S. Smith, Single-crystal elastic constants of lithium, *J. Phys. Chem. Solids* 9 (1959) 113–118.
- [54] M. E. Diederich, J. Trivisonno, Temperature dependence of the elastic constants of sodium, *J. Phys. Chem. Solids* 27 (1966) 637–642.
- [55] P. A. Smith, C. S. Smith, Pressure derivatives of the elastic constants of potassium, *J. Phys. Chem. Solids* 26 (1965) 279–289.
- [56] F. H. Featherston, J. R. Neighbours, Elastic constants of tantalum, tungsten, and molybdenum, *Phys. Rev.* 130 (1963) 1324–1333.
- [57] K. J. Carroll, Elastic Constants of Niobium from 4.2 to 300 K, *J. App. Phys.* 36 (1965) 3689–3690.

- [58] D. I. Bolef, R. E. Smith, J. G. Miller, Elastic properties of vanadium. I. Temperature dependence of the elastic constants and the thermal expansion, *Phys. Rev. B* 3 (1971) 4100–4108.
- [59] R. Gröger, J. Holzer, T. Kruml, Twinning and antitwinning in body-centered cubic metals (submitted manuscript), *Comp. Mater. Sci.*
- [60] T. Sedlatschek, J. Lian, W. Li, M. Jiang, T. Wierzbicki, M. Z. Bazant, J. Zhu, Large-deformation plasticity and fracture behavior of pure lithium under various stress states, *Acta Mater.* 208 (2021) 116730.
- [61] S. Küchler, V. Vojtech, S. S. A. Gerstl, R. E. Schäublin, J. F. Löffler, Thermally Decomposed Binary Fe–Cr Alloys: Toward a Quantitative Relationship Between Strength and Structure, *Adv. Eng. Mater.* 24 (2022) 2100909.
- [62] W.-Y. Chen, Y. Miao, J. Gan, M. A. Okuniewski, S. A. Maloy, J. F. Stubbins, Neutron irradiation effects in Fe and Fe–Cr at 300 °C, *Acta Mater.* 111 (2016) 407–416.

Curriculum Vitae



Jakub Holzer
holzer.jakub@gmail.com
(+420) 723 320 353
[Linkedin](#)

Work experience

- Application scientist** 8/2022 - present
Thermo Fisher Scientific Brno s.r.o.
Czech Republic
Application scientist
- Senior Intern** 11/2019 - 7/2022
Thermo Fisher Scientific Brno s.r.o.
Czech Republic
Application scientist
- Ph.D. Student** 9/2018 - 7/2022
Institute of Physics of Materials of Czech Academy of Sciences v.v.i.
Czech Republic
Group of Multiscale Modelling and Measurements of Physical Properties
- Visiting Researcher** 3/2021 - 4/2021
Paul Scherrer Institute
Switzerland
Laboratory for Neutron Scattering and Imaging
- Internship** 8/2020 - 10/2020
Paul Scherrer Institute
Switzerland
Laboratory for Neutron Scattering and Imaging
- Internship** 6/2018 - 8/2018
Paul Scherrer Institute
Switzerland
Laboratory for Nuclear Materials
- Master Student** 8/2016 - 5/2018
Institute of Physics of Materials of Czech Academy of Sciences v.v.i.

Czech Republic Low Cycle Fatigue Group Quality Control - Heat Treatment Division	Summers of 2014 - 2016
Swiss Steel s.r.o. Czech Republic Various summer jobs	5/2013 - 9/2013
United Kingdom	

Education

Doctor of Philosophy - Ph.D. Central European Institute of Technology Nanotechnology and Microtechnology	2018 - present
Master's Degree Brno University of Technology Faculty of Mechanical engineering Material Science	2016 - 2018
Bachelor's Degree Brno University of Technology Faculty of Mechanical engineering Material Science	2013 - 2016

Languages

Czech	Native speaker
English	Professional working efficiency
German	Elementary knowledge

Awards

Brno Ph.D. Talent Brno Municipality	2019
Sergio Marchionne Award CNH Industrial	2019

Projects

- CEITEC Specific research 2019 (CEITEC VUT-J-19-5955): Investigation of Anomalous slip in BCC metals using Transmission Electron Microscopy

Abstract

While plastic deformation of body-centered cubic (bcc) metals at low temperatures is now well understood, the effect of internal magnetic order on mechanical properties and the effect of plastic deformation of internal magnetic order remain largely unexplained. The aim of this thesis is to elucidate the low-temperature plastic deformation of α -iron and chromium with focus on magnetism. It is investigated by slip-trace analysis of deformed specimens, electron backscattered diffraction, and transmission electron microscopy (TEM) where necessary. The internal magnetic order in chromium is explored by means of magnetic neutron diffraction at SINQ facility of the Paul Scherrer Institute in Switzerland. The vibrating sample magnetometry is utilized to look for changes in mass susceptibility in order to discriminate between different magnetic states. The anomalous slip was found in a deformed chromium specimen for the first time. The dislocation network responsible for the anomalous slip is characterized by the $\mathbf{g} \cdot \mathbf{b}$ analysis in TEM, where a network of $1/2\langle 111 \rangle$ intersecting screw dislocations and their $\langle 100 \rangle$ junctions were observed to form on low-stressed $\{110\}$ planes. Furthermore, twins produced by antitwining shear were found in chromium, but not in α -Fe. This phenomenon is explained using atomistic simulations employing semi-empirical interatomic potentials. The magnetism in α -iron is studied by the vibrating sample magnetometry and the results are reconciled using the Jiles-Atherton model. The magnetic domains in α -Fe were imaged by the Kerr microscopy and the results show that twins can effectively block the movement of domain walls and nucleate new ones.